Research on Chemical Intermediates (2024) 50:2533–2560
https://doi.org/10.1007/s11164-024-05283-9

An appropriate approach and computational studies for evaluating metal shielding features using diazenyl naphthalen analogues as sustainable corrosion inhibitors

Selma Lamghafri[1] · Souheyla Chetioui[2,3] · Asma Barrahi[4] · Walid Daoudi[5] · Omar Dagdag[6] · Abdelmalik El Aatiaoui[5] · Avni Berisha[7] · Amel Djedouani[8,9] · Abdelkader Zarrouk[4] · Abdellatif Lamhamdi[1]

Received: 25 January 2024 / Accepted: 9 April 2024 / Published online: 6 May 2024

Abstract

The current work assessed the corrosion inhibitory efficacy of three ligands, namely methyl 2-((2-hydroxynaphthalen-1-yl)diazenyl)benzoate(MDN), 1-((3,4-dimethylphenyl)diazenyl)naphthalen-2-ol (DDN), and 3-((2-hydroxynaphthalen-1-yl)diazenyl)benzonitrile (HDN). Electrochemical and quantum methodologies, along with UV–Vis, SEM, and EDX, were employed. The anticorrosion process was comprehensively investigated. Potentiodynamic polarization validated the mixed type nature of inhibitors by demonstrating a drop in the cathodic hydrogen evolution reaction and the anodic metal dissolution, resulting to a significant decrease in corrosion current densities. Enhanced rates of effectiveness are achieved with higher inhibitor doses. Electrochemical impedance spectroscopy investigations confirmed the formation of a protective layer at the metal/solution interface, demonstrating that charge transfer was the primary cause of mild steel corrosion. The inhibitory potencies of the studied inhibitors at 10^{-3} M were 94.65, 94.56, and 93.63% for MDN, DDN, and HDN, respectively. The presence of several attributes in the molecular skeleton, such as nitrogen heteroatoms, aromatic rings, and the ester substituent group (CO_2CH_3), enhanced the availability of non-bonded and π-electrons and created stable covalent bonds by donating electrons to the iron surface. The inhibitory efficiency was better than 89% across all temperature ranges, suggesting the potential benefits of inhibitors at elevated temperatures. Adsorption trials revealed high effectiveness in corrosion control on mild steel, with Langmuir-based physisorption and chemisorption. The impact of electronegative O and N atoms, along with aromatic rings, in forming protective coatings was demonstrated by quantum chemistry computations which linked molecular structure and charge density patterns to the inhibition potency of MDN, DDN, and HDN, highlighting MDN's strong adsorption capacity.

Selma Lamghafri and Omar Dagdag have contributed equally to this work.

Extended author information available on the last page of the article

Keywords Corrosion products · Mild steel · Adsorption study · Physisorption

Introduction

In the industry, corrosion is a fatal problem which is due to the fact that corrosion problems account for a significant amount of the industry's annual budget, fatalities, and other detrimental social effects [1]. For instance, the oil and gas industry have numerous corrosion challenges which has increased dramatically in recent years. Rust is an inherent hazard in this refining sector, because of the impurities in crude oil that include a high sulfur content, hydrogen sulfide H_2S and CO_2 can harm dramatically pipelines and machine components causing pipe obstructions or mechanical damage to pumps and valves. Furthermore, corrosion caused by hydrochloric acid HCl and H_20 poses significant issues to equipment in atmospheric distillation operation. Corrosion is also a costly issue for many other industries that use metal, including manufacturing, chemical plants, aerospace, automotive, marine industry, etc. [2]. In this aspect, implementing effective corrosion control techniques can reduce the probability of these disasters. Copper corrosion inhibition is a topic of a great relevance due to its extensive application in numerous industrial process [3–5]. Due to its inexpensive cost and exceptional mechanical qualities, carbon steel is frequently used in industrial process [6]. However, in the presence of the acid corrosive medium, MS's resistance is significantly decreased. As these acidic ions are so corrosive, incorporating organic inhibitors into the cleaning solution are essential for reducing the rate of the steel corrosion [7]. Hydrochloric acid is the most common medium used in the industry; numerous studies have been performed included its application to steel [8]. Corrosion inhibitors were the most important anti-corrosion approach due to their ease of use and low cost. Thus, it is becoming crucial to generate organic molecules and research their potential as corrosion inhibitors. The application efficiently prevents mild steel from corroding in acidic solutions [9]. It significantly increases supply stability and has significant economic and social implications. Many chemical and inorganic corrosion inhibitors have been assessed [10]; nevertheless, the vast majority of these compounds are hazardous. Consequently, the use of inorganic corrosive agent became eventually curtailed [11]. Organic molecules with high electron density including heteroatoms such as (nitrogen, oxygen and sulfur), and aromatic rings double or triple bonds in their structures are more efficient [12], in fact the non-bonded electrons of the electronegative atoms and/or the π electrons of the cyclic ring interact with the d-orbital electrons of the iron atoms on the steel surface [13]. According to the literature, Inhibitors perform through adsorption via electron exchange to block the active sites on the metal surface and develop a layer covering the metal surface [14]. Moreover, organic molecule that are substituted by donor groups are better adsorbed on the considered surface resulting to the optimal preservation of the steel [15]. Recently, diazenyl naphthalen-based compounds have become a significant topic of chemical science research and development. Many studies have been conducted to investigate their performance as corrosion inhibitors. Amoko et al. [16] reported that steel subjected to hydrochloric acid environment demonstrated promising inhibition properties

using (E)-2-((2,5-dichlorophenyl) diazenyl) naphthalen-1-ol (DPD), in fact the presence of nitrogen atoms of the azo group, the oxygen atom of the substitute hydroxyl group, and the conjugated system were the primary active sites of DPD molecules that improved its adhesion on the steel surface. Akinyele et al. [17] confirmed that (E)-3-(2-(4-chloro-2-nitrophenyl)diazenyl)-1-nitrosonaphthalen-2-ol (CNN) exhibited a good inhibitory effect against 0.5 M HCl solution when applied, especially at large dosages. Akroujai et al. [18] conducted several tests to examine the anticorrosion properties of (E)-1-((4-fluorophenyl) diazenyl) naphthalen-2ol (E4FN), a maximum inhibitory efficiency of 94.8% was observed after inclusion of 10^{-3} M of (E4FN) to the solution. Obaid et al. [19] have discussed the possibility of mitigating corrosion in carbon steel. The results evinced excellent anticorrosion properties were displayed by the naphthalene compound. Fouda et al. [20] compared the inhibitory potency of [(5-mercapto-1H-1,2,4-triazole-3-yl)diazenyl] naphthalene-2-ol (HL) and its Mn complex, according to their findings, at 18×10^{-6} M the inhibition efficiency surpassed 90 and 85% for Mn complex and HL, respectively, concluding that the Mn complex is the most potent at avoiding steel corrosion.

The present research was carried out on mild steel specimen in the aim to investigate the inhibitory performance of three corrosion inhibitors, namely methyl 2-((2-hydroxynaphthalen-1-yl)diazinyl)benzoate (MDN), 1-((3,4-dimethylphenyl) diazinyl) naphthalen-2-ol (DDN), 3-((2-hydroxynaphthalen-1-yl)diazinyl)benzonitrile (HDN), By assessing the adsorption effect of ester, cyanide, and dimethyl groups on iron, comparing the anticorrosive properties of various organic ligands, and investigating the ligands' effectiveness as inhibitors for steel preservation. The peculiarity of this study is that it gives the current level of information on the excellent efficacy of naphthalene diazinyl compounds in inhibiting mild steel corrosion. The usage of these ligands has been decided according to a number of factors, including their high potential for corrosion inhibition, ease of synthesis from generally accessible raw materials, safety, and cost-effectiveness. The potency of these ligands was evaluated using both transient electrochemical techniques, such as electrochemical impedance spectroscopy (EIS), and stationary electrochemical techniques, such as potentiodynamic polarization (PDP). Theoretical framework and analytic surface approaches were used in supporting this finding.

Outlines of the investigation

Computational studies

Quantum chemical methods, and more specifically DFT, are increasingly used to describe molecular properties, comprehend the mechanism of action and forecast the effectiveness of inhibitors [21]. All quantum chemistry calculations and visualization of results were performed utilizing the software's Biovia Materials studio's Dmol3 module. Global optimizations are distinguished by the computation of vibration frequencies employing the DFT method are used to produce the researched compounds' geometric structure (using Dmol3, which included the SCAN/ DNP / COSMO (water) model) [22]. We conducted MC and MD simulations with the aid

of Materials Studio 8.0 software [23]. We apply the Fe (110) surface to simulate the adsorption mechanisms of the examined compounds on the Fe surface in this study. The simulation box used to carry out the molecular dynamics simulations has the dimensions (24.823752 × 24.823752 × 53.24658 Å). The iron slice and the number of water molecules comprising the studied compound associated with the simulation box. Before starting the simulation, the surface of Fe (110) and the molecular geometry of the compounds studied were optimized by minimizing the energies. Also, using the COMPASS III (Version 1.0) force field, MD simulations were run at 298 K with the NVT set, a time step of 1 fs, and simulation duration of 700 ps. This model comprised a Fe layer, 5 hydroniums, 5 chlorides, 730 H_2O molecules, 1 inhibitor molecule, and 40 vacuum layers in the simulation box.

Carbon steel and the aggressive medium

The chemical composition in % of the MS elements are distributed as follows: 99.6 iron, 0.16 carbon, 0.09 phosphorus, 0.05 sulfur, 0.02 manganese, chrome 0.05 and 0.03 aluminum, the coupon specimens were grinded using emery papers of different grit sizes going from 200 grade till 2000 grade then washed with distilled water after being degreased in acetone and finally left to dry in the air few minutes prior to use right after in the weight loss tests [24]. The corrosive medium was prepared by adding the commercially HCl with purity of 37% to the appropriate volume of distilled water. The three-diazenyl naphthalen analogues are presented in Fig. 1.

Electrochemical measurements

A potentiostat PGZ 402 programmed with Volta-Master 4 programming was used to conduct electrochemical experiments in a typical cylindrical Pyrex glass cell with three electrodes. Using saturated calomel electrodes (SCE) as reference electrodes and a platinum wire as a counter electrode, respectively. The steel samples were

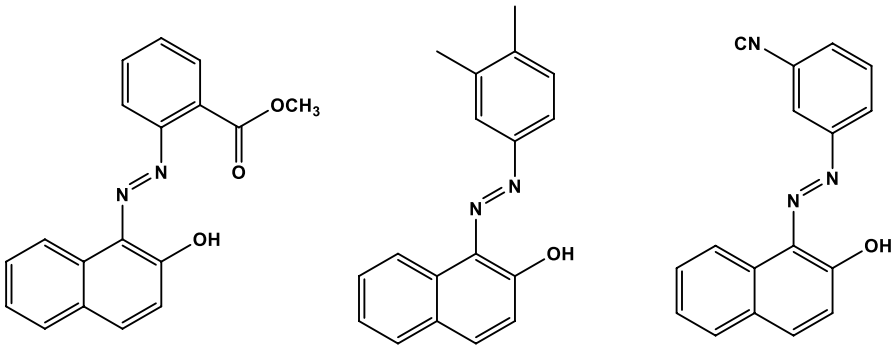

Fig. 1 MDN, DDN and HDN molecules

utilized as working electrode. The C-steel electrode was submerged in the corrosive electrolyte before measurements began. Following an immersion time of 1800s, the experiments were carried out in aerated solutions to allow the OCP values to stabilize. With a 10 mV perturbation, the frequency was shifted between 100,000 (high frequency) and 0.01 Hz (low frequency). Zview 2 was used to fit the EIS findings. The following expression provides the inhibitory potency (IE_{EIS}) generated from EIS.

$$IE_{EIS} = \left(\frac{R_P - R_P^0}{R_{P\cdot}} \right) \times 100 \quad (1)$$

where the terms R_p^o and R_P refer, respectively, to the polarization resistances in the blank and inhibited electrolytes. Tafel plots are scanned at a speed of 0.5 mV/s from − 800 to − 200 mV. EC-Lab V11.26 software was used to fit the polarization findings. The following equation provides the inhibitory capacity (IE_{PDP}) derived from polarization testing.

$$IE_{PDP} = \frac{\left(i_{corr}^o - i_{corr} \right)}{i_{corr}^o} \times 100 \quad (2)$$

The corrosion current densities in the blank and inhibited electrolytes, respectively, are denoted by the letters i_{corr} and i^0_{corr}, respectively.

Surface investigation

The above-described process was followed to prepare the steel specimens, which were then submerged for 24 h in 1 M HCl with and without the chosen inhibitor at the optimal dose. The samples were then subjected to SEM analysis coupled with X-ray EDS micrographs in order to examine the coupon surface photographs, assess the surface topography, and provide detailed information about its constituents, also employing a Jasco V-730 spectrophotometer; UV–visible wavelengths have been used to reveal more information on complex development (inhibitor-Fe).

Results and discussion

Theoretical analysis

DFT results

The optimized structures of the investigated molecules, HDN, DDN and MDN compounds are examined. These molecules exhibit potential as effective inhibitors for safeguarding metal surfaces against corrosion, given their abundance of oxygen and nitrogen atoms, including carbonyl, hydroxyl oxygen's, and diazine, attributed to the π-electrons within the aromatic rings. Figure 2 illustrates the optimized structures,

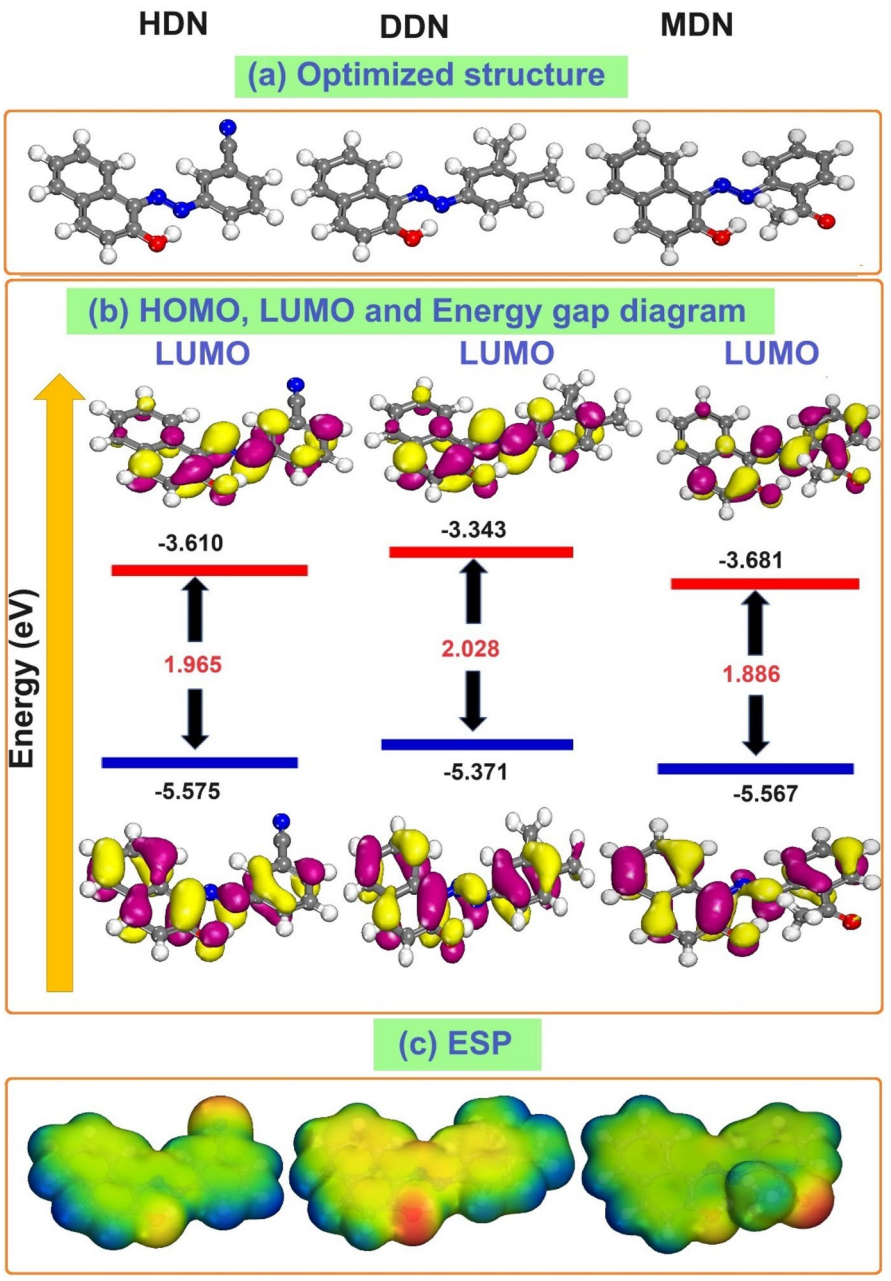

Fig. 2 Optimized structures, HOMO, LUMO and ESP pictures of HDN, DDN and MDN compounds

HOMO and LUMO surfaces, energy gap diagrams, and ESP maps of the investigated inhibitors. The HOMOs and LUMOs are spread throughout the majority of the skeleton of HDN, DDN, and MDN compounds, according to an examination of

Fig. 2, which illustrates the distribution of total density mapped with the electrostatic potential, further validates the findings (MEP). The progressive decrease in electron density is depicted by the gradient of colors, transitioning from red to blue. E_{HOMO} signifies a molecule's inclination to donate electrons to an acceptor species, while E_{LUMO} characterizes an inhibitor's predisposition to accept electrons from a donor molecule [25]. Prior research indicates that higher E_{HOMO} values enhance the adsorption ease of molecules on a metal surface, and lower E_{LUMO} values correlate with better inhibition potential. Conversely, the energy gap, representing the difference between E_{LUMO} and E_{HOMO}, relates to the energy barrier that must be overcome for inhibition [26]. Furthermore, ΔE, associated with the molecule's reactivity, is inversely proportional; more reactive molecules exhibit lower ΔE (fundamental gap) values, and vice versa [27].

Reviewing Table 1 reveals an E_{HOMO} trend for HDN, DDN, and MDN inhibitors: DDN (− 5.371 eV) > MDN (− 5.567 eV) > HDN (− 5.575 eV). This suggests that the DDN molecule has a slightly greater inclination to donate electrons to the vacant d-orbitals of Fe compared to the HDN and MDN molecules. Conversely, the E_{LUMO} ranking for the investigated inhibitors is as follows: MDN (− 3.681 eV) < HDN (− 3.610 eV) < DDN (− 3.343 eV). This implies that the MDN molecule, characterized by a lower E_{LUMO} value, possesses a greater capacity to accept electrons from the Fe surface, indicating potential back-donation interactions. The MDN (1.886 eV) exhibits a marginally smaller ΔE value than HDN (1.965 eV) and DDN (2.028 eV), suggesting a slightly stronger influence of the [Fe—MDN] complex in comparison with [Fe—HDN] and [Fe—DDN]. η and σ are two crucial characteristics that assess a molecule's stability and reactivity. Table 1 also displays the computed values of η and σ. The literature reveals that a soft molecule has a small ΔE_{gap} [11], on the one hand, and on the other, the high corrosion-inhibiting efficiency of a molecule is linked to a low value of η and a high value of σ [28]. According to the η and σ parameters of the inhibitors examined (Table 1), it is quite clear that the MDN inhibitor has the lowest η value (0.943 eV) and the highest σ value (1.060 eV), this result explains its high efficiency compared to HDN and MDN. These observations are

Table 1 The computed quantum chemical descriptors for HDN, DDN and MDN compounds

Theoretical parameters	HDN	DDN	MDN
E_{HOMO} (eV)	− 5.575	− 5.371	− 5.567
E_{LUMO} (eV)	− 3.610	− 3.343	− 3.681
ΔE (E_{HOMO}—E_{LUMO}) (eV)	1.965	2.028	1.886
I (eV)	5.575	5.371	5.567
A (eV)	3.610	3.343	3.681
χ (eV)	4.592	4.357	4.624
η (eV)	0.982	0.970	0.943
σ (eV^{-1})	1.018	1.031	1.060
ΔN	0.116	0.238	0.104
$\Delta E_{back\text{-}donation}$	− 0.245	− 0.242	− 0.235

consistent with experimental results. The outcome of $\Delta E_{back\text{-}donation}$ suggests that when $\eta > 0$ or $\Delta E_{back\text{-}donation}$, back-donation from the phytochemical to the metal surface is energetically favored. The results presented in Table 1 indicate that $\Delta E_{back\text{-}donation}$ is true; consequently, the anticipated inhibition efficiency follows the sequence MDN > DDN > HDN.

Utilizing MAC allows for a precise and dependable assessment of the inhibiting sites (atoms) engaged in the metal absorption process. The analysis of these data can facilitate the generation of the metal absorption prediction. Numerous hypotheses have been put forward to elucidate the increased likelihood of interaction between a particular atom on the surface of Fe (110) and various inhibitory compounds. These hypotheses aim to provide insights into this observed phenomenon [29]. According to Fig. 3, the most negative charges of the both molecules, and are located on atoms N, C and O. According to this finding, these atoms are most likely the active adsorption centers.

MC and MD simulations

Commencing the computation of the adsorption energy for the system with the Fe(110) surface significantly streamlines the calculation process. Building upon the previous step, it is now possible to ascertain the adsorption energies of the system [30]. For the computation of the adsorption energy (E_{ads}) of a molecule on the Fe(110) surface, the following equation is employed:

$$E_{ads} = E_{Fe(110)//inhibitor} - \left(E_{Fe(110)} + E_{inhibitor}\right) \tag{3}$$

Following the successful completion of Monte Carlo (MC) computations, as depicted in Fig. 4, thorough investigations were undertaken on the adsorption geometry of the inhibitor to validate the accuracy of the results [31]. Evaluating the equilibrium in the Monte Carlo (MC) simulation involves comparing the energy values at the steady state with those at the simulation's initiation, thereby discerning the difference between the two sets of values. This comparison is made by contrasting the energy values at the steady state with those at the beginning of the simulation. At this juncture, the simulation had advanced to a stage where the system functioned with the minimal energy required to sustain its movement[32].

At this point, the system had not only completed the simulation but had also entered a state where it maintained forward motion with the minimal necessary energy. The active state of the adsorbent inhibitors is illustrated in Fig. 4, highlighting the specific configuration that defines their condition. Within the Molecular Dynamics (MD) technique, the inhibitor aligns itself on the surface of Fe (110) in a manner closely parallel to its optimal positioning, emphasizing contact with its oxygen and nitrogen atoms. This configuration ensures the most robust connection with these atoms [33]. Consequently, an optimal level of interaction is established between the inhibitor and these atoms. Figure 4 illustrates an adsorption pattern conceptualized by our group, attributing it to the inclination of the inhibitor molecule's backbone to attach to the surface atoms of the Fe (110) plane. The figure visually represents this pattern. The credibility of this

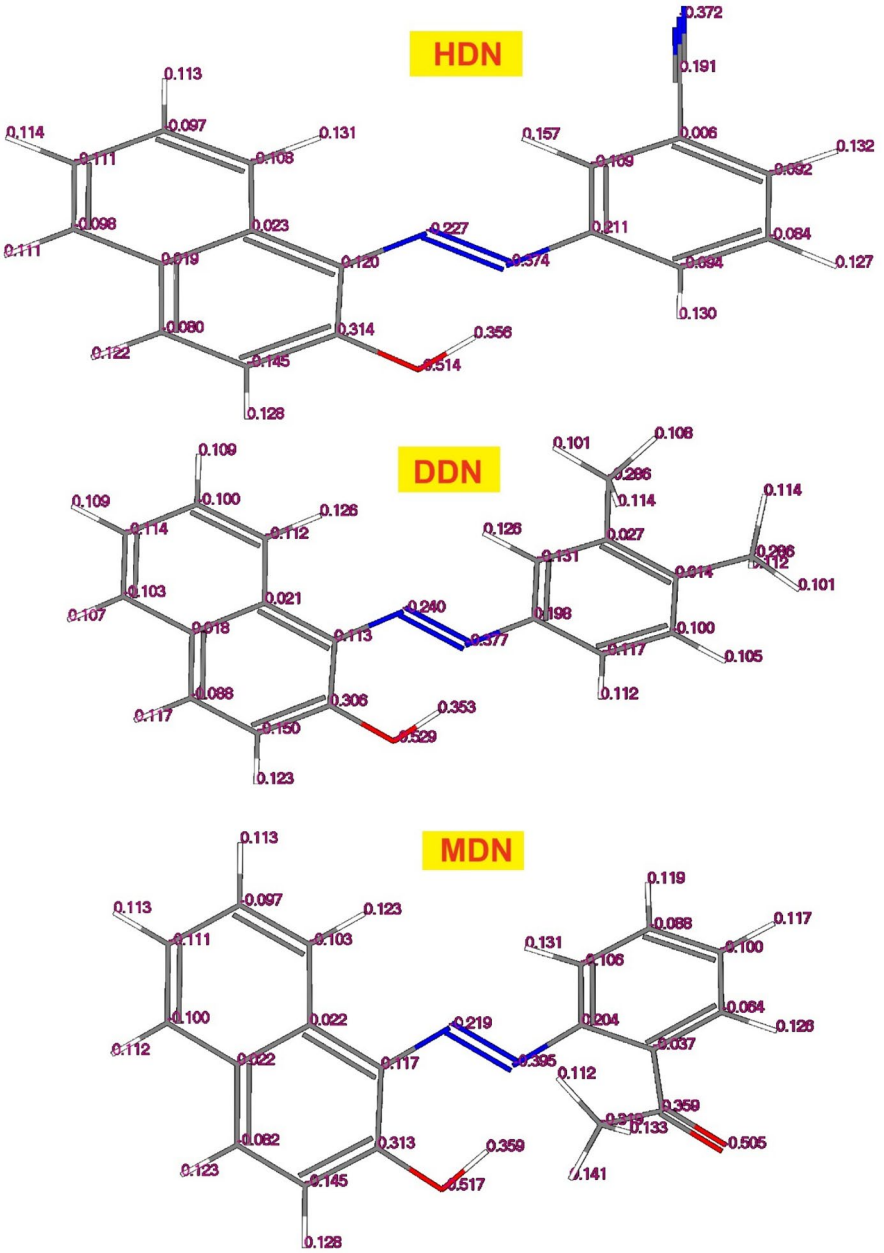

Fig. 3 Mulliken atomic charge distribution for HDN, DDN and MDN compounds

hypothesis is reinforced by accumulated information, given that these specific molecules exhibit a tendency to bring their heteroatoms (O and N) and electron rings closer to the surface, facilitating adsorption. The distinctive properties of

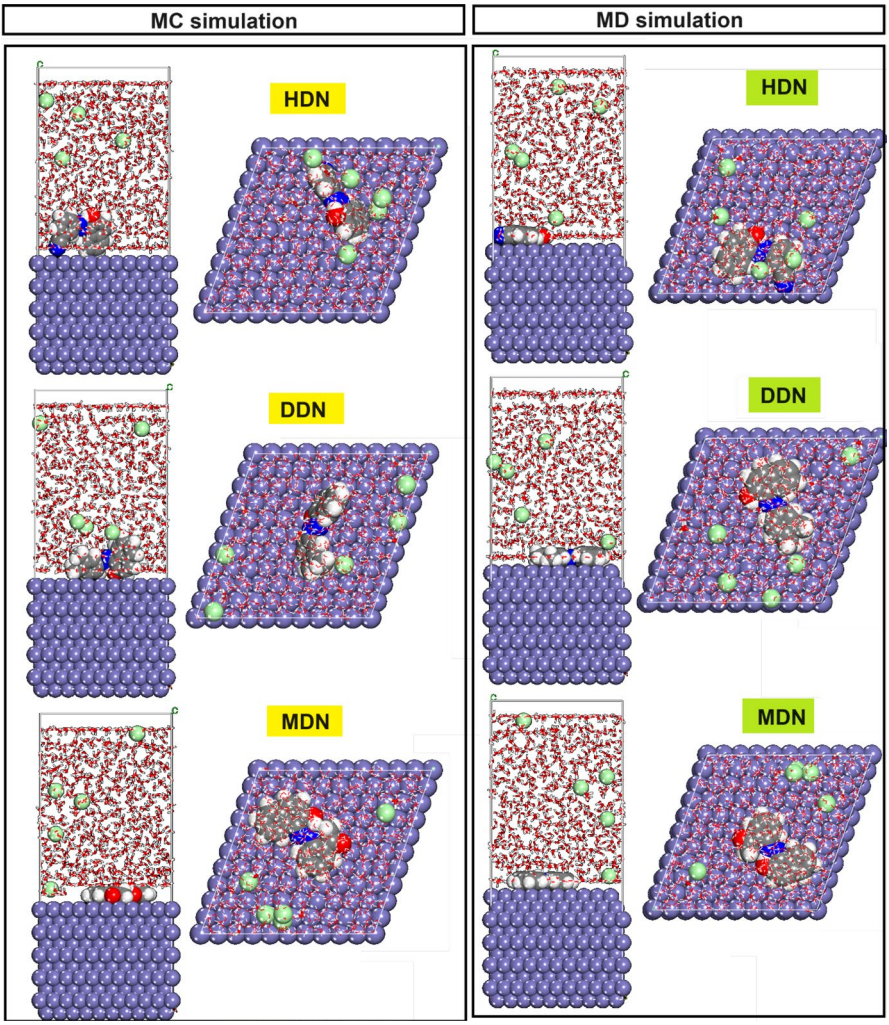

Fig. 4 MC and MD simulations results: setups and adsorption positions of HDN, DDN and MDN compounds on the Fe(110) surface

these molecules stem from their ability to transport heteroatoms and electron rings in proximity to the surface, enabling them to absorb other molecules [34].

The adsorption energies observed for the inhibitors on metal surfaces are notably high, as illustrated in Fig. 5. These elevated adsorption energies indicate a significant adsorptive interaction between the inhibitor molecules and the metal surface. The interactions, particularly those involving the HDN, DDN, and MDN compounds, present a novel approach for establishing a protective layer on the metal surface. This protective layer serves as a shield, effectively safeguarding the metal from corrosion. According to these results, the order of inhibitory potency

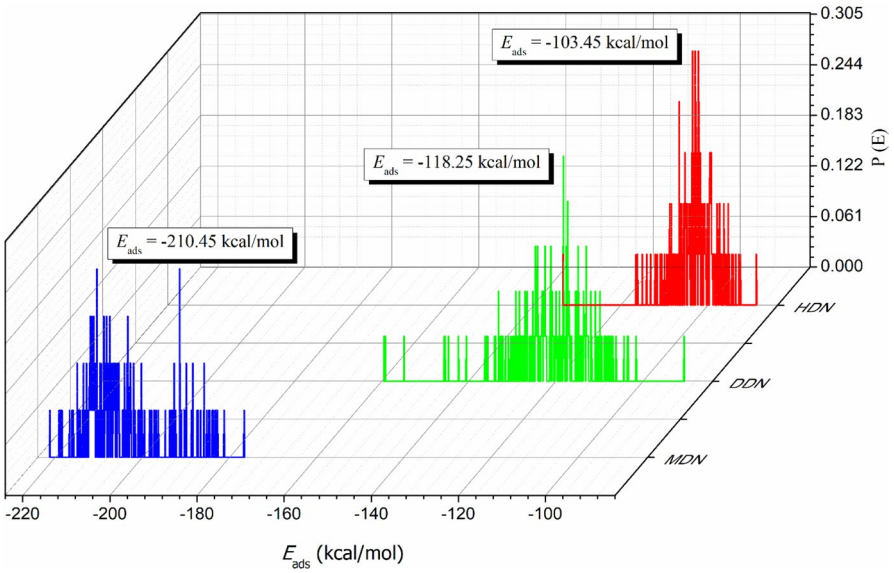

Fig. 5 Distribution of the E_{ads} of the HDN, DDN and MDN inhibitors onto the Fe surface obtained by via MC

of HDN, DDN and MDN compounds is as follows: MDN ($E_{ads} = -210.45$ kcal/mol) > DDN ($E_{ads} = -118.25$ kcal/mol) > HDN ($E_{ads} = -103.45$ kcal/mol).

The RDF derived from the MD trajectory in corrosion simulations is presented in a format designed for easy comprehension. This presentation seeks to enhance understanding of the physisorption and chemisorption processes occurring during the adsorption of corrosion inhibitors on the Fe(110) surface [35]. The MD trajectory examines the radial distribution function of heteroatoms in HDN, DDN, and MDN compounds on Fe(110). Peaks observed in the RDF graphs at various distances from the metal surface indicate the nature of adsorption activity occurring on the metal surface. The chemisorption technique is utilized when the peak height falls within the range of 1 to 3.5 Å, while the physical adsorption method is employed when the peak is observed at a distance beyond 3.5 Å. The projection of RDF peaks is consequently anticipated at distances exceeding 3.5 Å, as illustrated in Fig. 6. The peak RDF values for oxygen (O) and nitrogen (N) atoms occur when the distance is within 3.5 Å for HDN, DDN and MDN compounds. This suggests close proximity between the inhibitors and the Fe(110) surface.

Potentiodynamic polarization (PDP)

The Tafel polarization approach was utilized to further comprehend the kinetics of cathodic and anodic region in 1.0 M HCl. Figure 7 displays the polarization plots of C-steel in 1.0 M HCl solution containing and without the introduction of different doses of MDN, HDN, and DDN inhibitors.

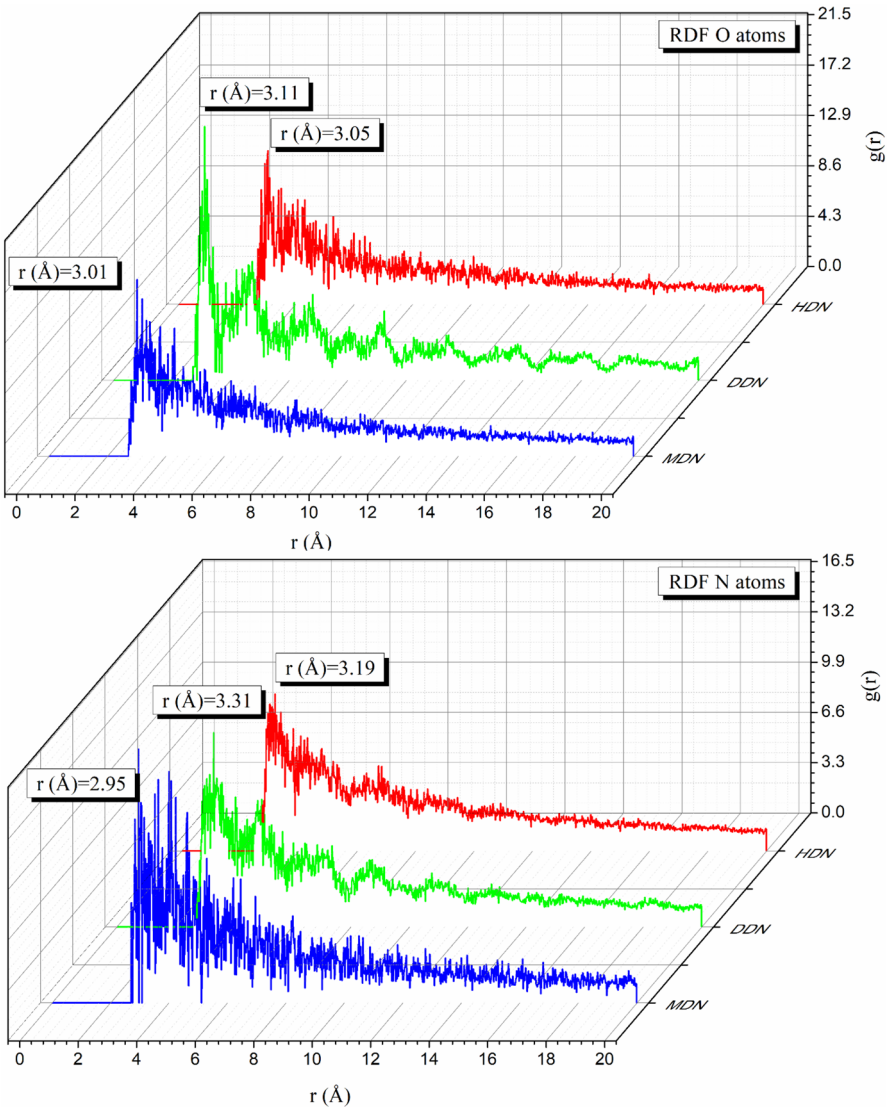

Fig. 6 RDF O and N atoms of the HDN, DDN and MDN inhibitors in the simulated corrosion media onto Fe surface obtained via MD

It is clear from the (PDP) curve analysis that MS inhibition in 1 M HCl becomes more pronounced as the concentration of inhibitors increases. Additionally, it is evident that the presence of the ligands slows down the cathodic hydrogen evolution and anodic metal dissolution reactions. The current densities are consequently noticeably lower, demonstrating that the corrosion reaction has been suppressed following the addition of the investigated inhibitor [35]. Table 2 shows that the i_{corr} value reduces noticeably as the concentrations of MDN, HDN, and DDN are increased.

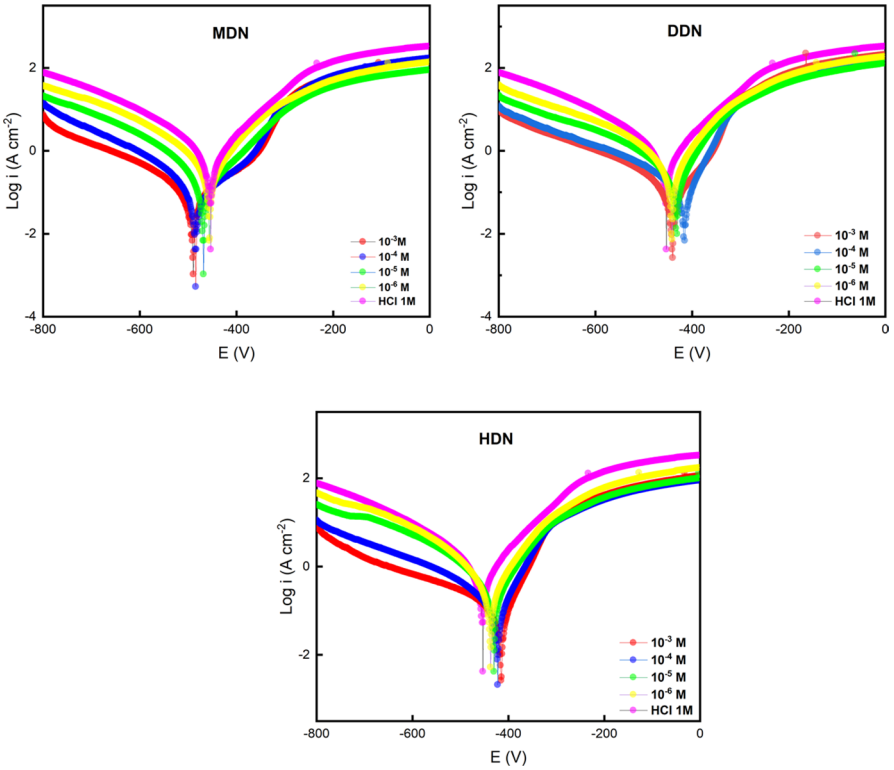

Fig. 7 Polarization plots of C-steel in 1.0 M HCl solution

Table 2 Tafel parameters derived from PDP curves

Comp	Conc. (M)	$-E_{corr}$ (mv/SCE)	I_{corr} (μA/cm^2)	$-\beta c$ (mv.dec^{-1})	βa (mv.dec^{-1})	IE_{PDP} (%)
Blank	1	456.3	1104.3	112.8	155.4	-
MDN	10^{-3}	489.0	59.0	105.8	117.1	94.6
	10^{-4}	484.5	72.6	96.2	124.7	93.4
	10^{-5}	468.2	181.0	112.1	102.9	83.6
	10^{-6}	454.9	320.9	111.1	85.4	70.9
DDN	10^{-3}	439.2	59.8	85.5	71.0	94.5
	10^{-4}	415.0	87.3	123.0	50.8	92.0
	10^{-5}	431.5	181.1	107.0	60.6	83.5
	10^{-6}	441.0	246.2	91.3	64.6	77.7
HDN	10^{-3}	414.9	70.3	139.4	50.9	9 3.6
	10^{-4}	421.9	104.4	136.0	59.5	90.5
	10^{-5}	429.5	237.2	105.0	74.0	78.5
	10^{-6}	436.3	366.3	110.1	82.6	66.8

The i_{corr} is elevated for 1.0 M HCl solution (1104.3 µA /cm^2), but it is lower for MDN (59.008 µA /cm^2), DDN (59.884 µA /cm^2), and HDN (70.327 µA /cm^2) at the amount 10^{-3} M of inhibitors. Additionally, the fluctuation of the corrosion potential is strictly inferior to 85 mV for all inhibitors, confirming the mixed type nature of the examined inhibitors [36]. The presence of inhibitors has also resulted in a minor alteration of the cathodic and anodic Tafel slopes. The slopes of the anodic Tafel lines show that the inhibitors under study was initially adsorbed into the iron interface and hindered the reactivity sites without modifying the anodic reaction mechanism [37]. Additionally, the inclusion of organic molecules slightly modifies the ligands' βc values, showing that the reaction involving hydrogen evolution is slowed down [38], this outcome can be explained by the covering of active sites brought on by the adhesion of the inhibitor molecules [39]. In addition, it is evident that diazenyl naphthalen analogues increase the inhibitory effectiveness, reflecting the fact that the metallic surface coating expands as concentration rises [40]. The inhibitory potency of the investigated inhibitors at 10^{-3} M was 94.65, 94.56, and 93.63% for MDN, DDN, and HDN, respectively. The MDN inhibitor value was found to be the highest, the presence of several attributes in the molecular skeleton, namely nitrogen heteroatoms, aromatic rings, and the ester substituent group (CO_2CH_3), enhance the availability of non-bonded and π-electrons and can create stable covalent bonds by donating electrons to the iron surface [41], improving the organic molecule's ability to adhere to the metallic surface. As a result, MDN molecule exhibit the highest potent inhibitor efficacy of steel corrosion [42].

Electrochemical impedance studies

The metal/solution interface processes were described using the electrochemical impedance (EIS) technique, which highlights the fundamental and complicated mechanisms. This approach is specifically designed to identify the inhibitory compounds' mode of action, allowing evaluation of the produced film's dielectric properties [43]. Mild steel experiments (EIS) in molar hydrochloric acid were assessed in the existence and without various inhibitor doses varying from 10^{-3} to 10^{-6} M, Bode and Nyquist plots are displayed in Figs. 8, 9, respectively.

Visual analysis of Nyquist curves showed a single capacitive loop with identical shape. This indicated that the charge transfer is mainly responsible for the carbon steel's resistance to dissolve in 1 M HCl solution [44]. Additionally, as the concentration of the organic chemicals increased, the semi-circle's diameter grew. According to this, the inclusion of inhibitor molecules did not result in any significant changes to the corrosion mechanism [45]. According to the Bod and phase plots, it is evident that when ligands concentration rise, the values of the phase angle also rise and are higher in the presence of the chosen inhibitors than the blank results. These findings show the protective effect of MDN, DDN and HDN in the oxidation process of mild steel [46]. the phase angles are also less than 90°, emphasizing even more the non-ideal performance of these systems (CPE) resulting of the interfacial impedance's frequency dispersion caused by the MS surface's heterogeneity and roughness [47]. A single phase angle maximum indicates

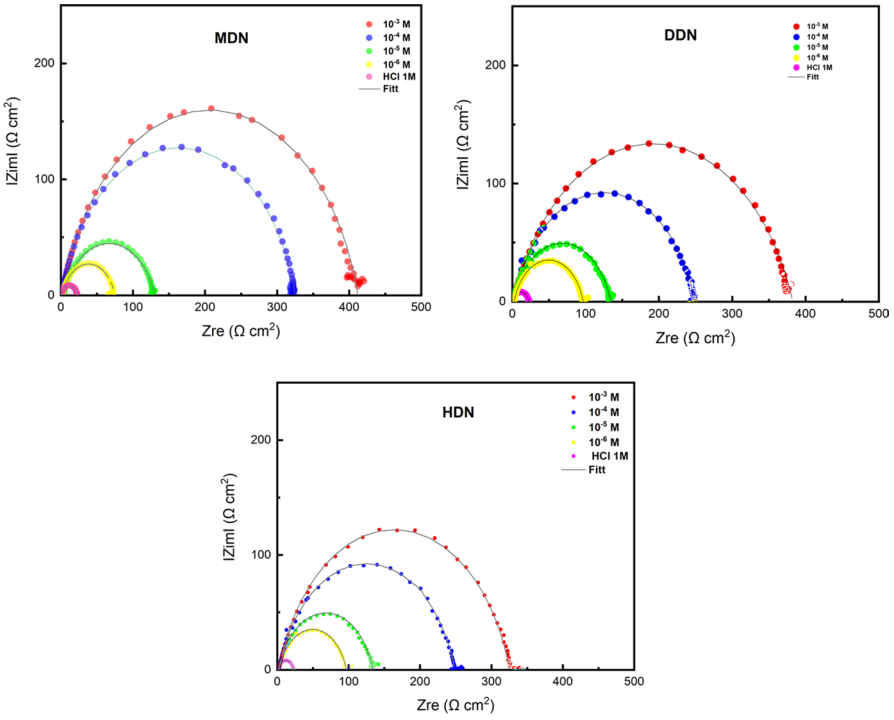

Fig. 8 Nyquist plots of C-steel in 1.0 M HCl solution

that there is only one time constant, and as a result, only one relaxation process has occurred during the charge transfer process [48]. Using the suitable circuit shown in Fig. 10, the experimental impedance and Bode curves were adjusted for the three components. The electrolytic resistance (Rs), the polarization resistance (R_p), and the constant phase element (CPE/n_{dl}) derived from the non-ideal capacitive conduct of the electronic double layer are the three fundamental components of this electrical circuit [49]. Table 3 includes the retrieved and computed parameter values. The information presented in the table shows that, when MDN, DDN, and HDN are added, the value of R_p raised in comparison with the blank solution, this rise in R_p value is ascribed to the development of a protective coating at the metal/solution interface [50], also a lowering in C_{dl} values may be brought on by a drop in the local dielectric constant or a thickening of the electrical double layer [51], indicating that inhibitory molecules are adsorbing at the metal/solution interface favoring the generation of adsorptive films on metallic interfaces enhancing the effectiveness of inhibition [52]. The percentage of the C-steel that was inhibited in the presence of substantial amounts of MDN, DDN and HDN was 94.7, 94.3, and 93%, respectively. The higher sorption of MDN may be attributed to the molecule's high reactivity at the metal/solution interfaces of the group, including functional ester (CO_2CH_3) [53].

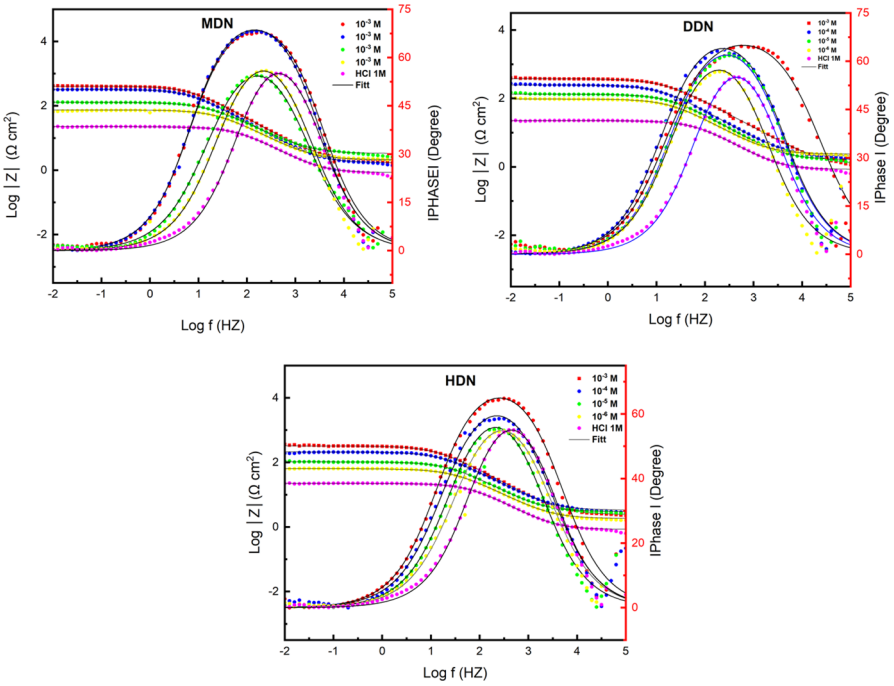

Fig. 9 Bode and phase plots of C-steel in 1.0 M HCl solution

Fig. 10 Suitable electrical circuit describing the evaluated system

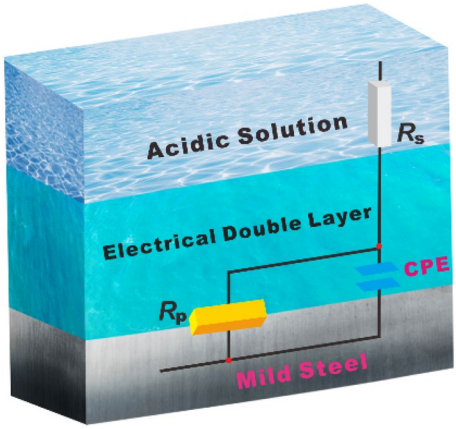

Temperature effect and activation parameters

Temperature may affect the procedure of interaction between C-steel and inhibitors in an acidic medium [54]. In order to determine the effect of temperature impact on the corrosion rate and metal deterioration PDP measurements were carried out

Table 3 Electrochemical parameters derived from EIS curves

Comp	Conc. (M)	R_s (Ω cm^2)	R_p (Ω cm^2)	C_{dl} (μF cm^{-2})	Q ($\mu Fcm^{-2}S^{n-1}$)	n_{dl}	IE_{EIS} (%)	$\chi^2.10^{-3}$
HCl	1	0.85 ± 0.01	21.59 ± 0.01	120.3	309.38 ± 0.01	0.841 ± 0.006	–	2 .2
MDN	10^{-3}	2.12 ± 0.05	407.11 ± 0.31	46.6	75.01 ± 0.01	0.880 ± 0.001	94.7	8.9
	10^{-4}	1.72 ± 0.05	322.99 ± 0.03	74.4	129.85 ± 0.01	0.850 ± 0.001	93.3	1.03
	10^{-5}	3.29 ± 0.04	127.01 ± 0.02	79.2	214.45 ± 0.01	0.783 ± 0.002	83	1.24
	10^{-6}	2.14 ± 0.01	72.72 ± 0.04	87.5	222.14 ± 0.02	0.815 ± 0.001	70.2	0.04
DDN	10^{-3}	1.03 ± 0.03	381.51 ± 0.21	27.9	76.26 ± 0.03	0.779 ± 0.002	94.3	2.12
	10^{-4}	2.05 ± 0.02	246.69 ± 0.28	51.9	114.35 ± 0.03	0.818 ± 0.005	91.2	7.4
	10^{-5}	1.62 ± 0.01	132.51 ± 0.09	63.6	151.38 ± 0.02	0.818 ± 0.002	83.6	2.99
	10^{-6}	2.36 ± 0.02	94.36 ± 0.01	84.8	203.95 ± 0.02	0.818 ± 0.003	77.1	2.81
HDN	10^{-3}	2.41 ± 0.01	322.80 ± 0.06	37.7	81.56 ± 0.02	0.824 ± 0.004	93.3	2.91
	10^{-4}	3.31 ± 0.02	209.01 ± 0.04	44.3	109.77 ± 0.01	0.806 ± 0.027	89.6	1.56
	10^{-5}	2.99 ± 0.02	101.81 ± 0.03	65.1	164.11 ± 0.06	0.815 ± 0.011	78.7	8.13
	10^{-6}	1.82 ± 0.02	62.19 ± 0.02	81.0	229.69 ± 0.04	0.803 ± 0.063	65.2	2.42

between 303 and 333 K before and after adding 10^{-3} M of the investigated inhibitors as shown in Fig. 11.

The findings demonstrated that, in the presence of inhibitors, corrosion rate increased very marginally as temperature intensified. This demonstrates that chemical adsorption of the ligands entails powerful interactions between the investigated inhibiting compounds and metal surface, is mainly responsible for controlling the dissolution of metal [55]. Referring to the Table 4, it is clear that the rise of temperature leads to an increase in the corrosion rate for both the inhibited and uninhibited acidic solution, consequently the inhibitory efficiency decreases, it goes from 94.65 to 91.2% for MDN, 94.5 to 91.1% for DDN and from 93.6–90.3% for HDN in the studied temperature range. This observation implies that MDN, DDN, and HDN molecules demonstrate modest separation from the metal surface as the temperature exceeds 333 K, indicating that the temperature has a minor impact on the carbon steel corrosion in the aggressive solution causing the dissolution of the metal [56]. It can also be noticed that the inhibitory efficacy values for the MDN inhibitor diminishes gradually as temperature increases. This behavior can be explained by the lowered desorption of MDN molecules from the surface of mild steel compared to HDN and DDN [48]. On the contrary, EI_{PDP} (%) values for the HDN compound decrease with increasing temperature, indicating a significant degree of mild steel dissolving. These findings suggest that MDN is more robust to temperature rise than HDN and DDN. This validates earlier findings that the ester (CO_2CH_3) group in the MDN structure favorably impacts inhibitory behavior by boosting its inhibitory efficacy. Moreover, the inhibitory power for the three inhibitors (from 303 to 333 K) remains higher than 90% indicating that the examined inhibitors are efficient for applications involving high temperatures [57]. As a result, it is possible to conclude that the adsorption process is predominantly controlled by chemical interactions between the reactive sites of the diazinyl-naphthalen molecules and the metal

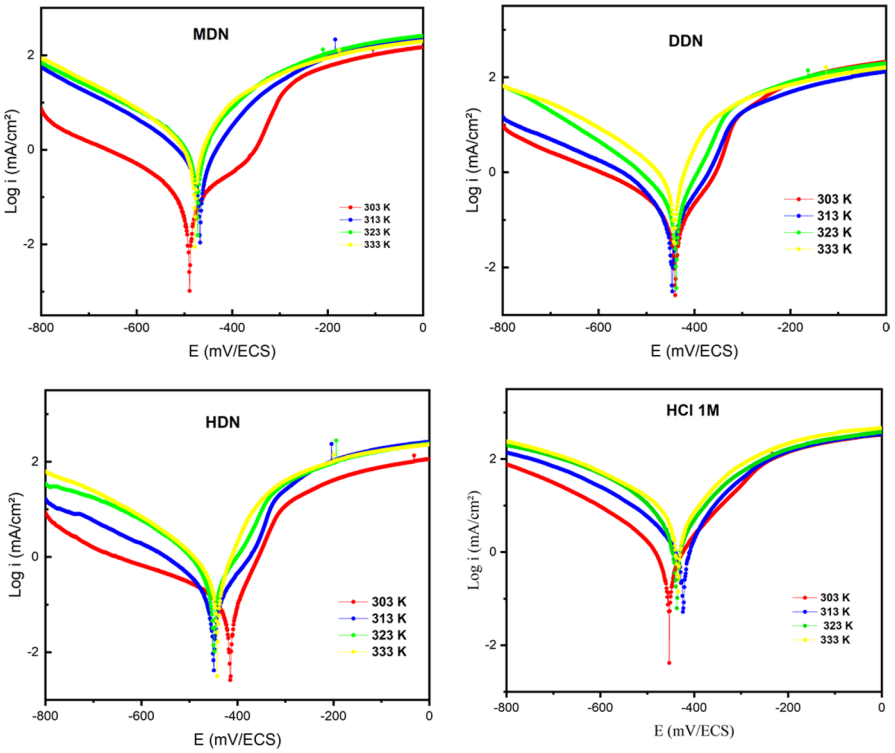

Fig. 11 Tafel temperature plots of C-steel in 1.0 M HCl solution

Table 4 Temperature parameters derived from PDP curves

Compounds	Temperature (K)	$-E_{corr}$ (mVvs CSE)	i_{corr} (μA/cm^2)	$-\beta_c$ (mV/dec)	β_a (mV/dec)	IE_{PDP} (%)
MDN	303	489.0	59.0	105.8	117.1	94.6
	313	467.2	96.4	28.1	31.5	93.4
	323	473.4	195.9	30.1	26.6	91.3
	333	477.5	422.4	68.4	46.6	91.2
DDN	303	439.2	59.8	85.5	71.0	94.5
	313	446.7	96.8	108.0	72.1	93.4
	323	439.1	162.4	94.1	54.9	92.7
	333	442.1	350.1	85.5	47.7	91.1
HDN	303	414.9	70.3	139.4	50.9	9 3.6
	313	449.3	111.8	96.8	81.4	92.4
	323	448.2	190.9	72.1	65.7	91.5
	333	441.7	380.4	116.2	60.0	90.3

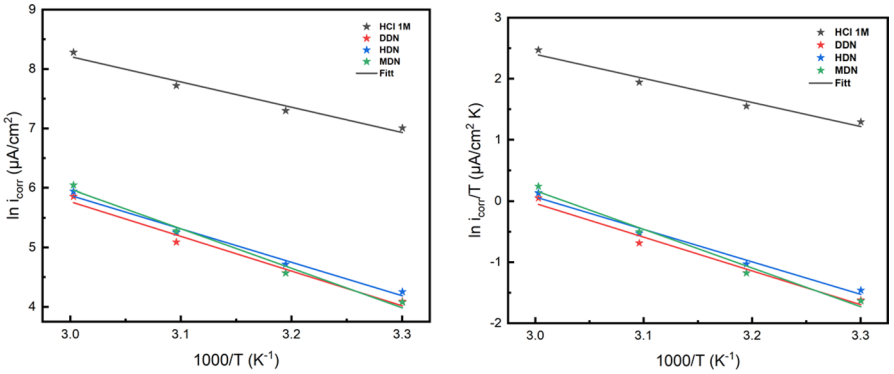

Fig. 12 Arrhenius lines of C-steel in 1.0 M HCl solution

Table 5 Activation parameters derived from Arrhenius lines

Compounds	R^2	E_a* (KJ/mol)	ΔH_a* (KJ/mol)	ΔS_a* (J/mol.K)	$E_a^* - \Delta H_a^*$ (kJ/mol)
Blank	0.97177	35.42	32.78	-79.23	2.64
MDN	0.97708	55.30	52.66	-38.11	2.64
DDN	0.96966	48.60	45.96	-59.96	2.64
HDN	0.97889	46.82	44.18	-64.39	2.64

substrate [9]. Activation parameters are influenced by temperature, in fact numerous investigations have demonstrated that the expansion of the metal surface that the inhibitor molecules are covering following their addition to the acidic solution is the reason causing diminution of the activation energy (E_a*) as shown in Arrhenius equation [58] (Fig. 12).

$$ln\left(i_{corr}\right) = ln(\mathrm{A}) - \frac{\mathrm{E}_a^*}{\mathrm{RT}} \tag{4}$$

where *A* is the Arrhenius constant and *R* is the universal perfect gas constant. The plot of $\ln(i_{corr})$ versus 10^3/T shows straight line of which $-(E_a^*)/R$ is the slope that enables us to determine the activation energy.

According to Table 5**,** the activation energy value of the blank solution is of the order of 35.42 (KJ/mol) indicating the energy hurdle that inhibitor must overcome in order to adsorb onto the surface of the substrate [59]. Straight line obtained from the plot $\ln(i_{corr}/T)$ versus $10.^3$/T allowed us to determine the enthalpy (ΔHa*) and the entropy (ΔSa*)using the Arrhenius transition state relation: [60]

$$ln\left(\frac{i_{corr}}{\mathrm{T}}\right) = [ln\left(\frac{\mathrm{R}}{\mathrm{Nh}}\right) + (\frac{\Delta \mathrm{S}_a^*}{\mathrm{R}})] - \frac{\Delta \mathrm{H}_a^*}{\mathrm{RT}} \tag{5}$$

where *h* is the Planck constant and *N* is the number of Avogadro. According to the table we can notice that the (Ea*) value of MDN is the highest compared with DDN

and HDN inhibitors indicating the greatest inhibitory effectiveness [61]. The endothermic aspect of the steel corrosion is indicated by the positive sign of the enthalpy (ΔH_a^*) while the negative sign of the entropy(ΔS_a^*) reveals the growth of an inhibitor layer on the surface of the steel [62].

Adsorption parameters

The displacement of the original adsorbed water molecules occurs during the adsorption of the investigated diazenyl naphthalen compounds on the carbon steel surface [63]. The substitution happened because the energy occurring between organic compounds and metal surfaces was higher than the energy of interaction between water molecules and interfaces [64]. Additionally, to decide which adsorption isotherm type fits the best, a number of isotherms have been investigated to describe the interaction between molecules and the metallic surface such as Langmuir [65], Temkin [66], Frumkin [67], and Freundlich [68].

According to the calculated linear regression coefficients (R^2) in Fig. 13, the Langmuir adsorption isotherm model accurately predicted the adsorption of organic molecules on carbon steel's surface, allowing us to determine the equilibrium constant for adsorption (K_{ads}) of the ligands on the surface of carbon steel utilizing the following formula [69].

$$\Delta G_{ads} = -RT ln\left(k_{ads} \times 55.5\right) \tag{6}$$

The absolute temperature is denoted by T, whereas R stands for the universal gas constant while 55.5 M is the concentration of water in solution [70]. The thermodynamic parameters are gathered in Table 6.

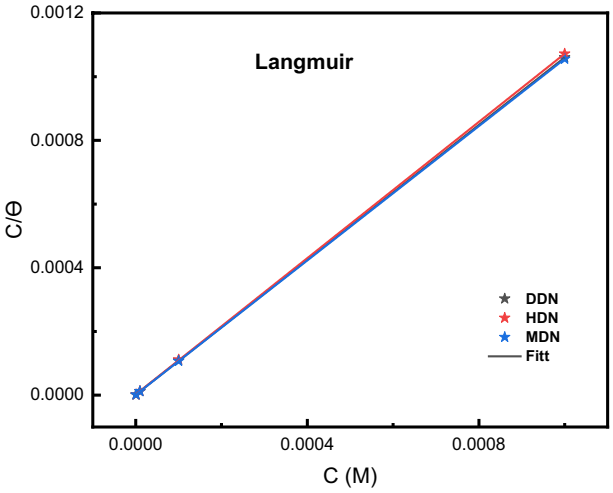

Fig. 13 Langmuir lines of the concerned system

Table 6 Langmuir isotherm parameters of the concerned system

Molecules	R^2	$K_{ads} \times 10^3$	Slope	ΔG_{ads}(KJ/mol)
MDN	1	849.062	1.05453	−44.508
DDN	0.99999	583.012	1.05859	−43.561
HDN	0.99998	441.920	1.06977	−42.863

The negative values of ΔG_{ads} explain the spontaneous adsorption of MDN, DDN and HDN molecules on the surface of carbon steel, the fact that for the three inhibitors ΔG_{ads} values are greater than 40 kJ mol^{-1} indicates that there are strong contacts between the steel surface and inhibitors [71], which are adsorbable by strong coordinate covalent bonds (chemisorption) [72].

UV–Vis investigation

To find out more about complex formation (inhibitor-Fe), UV–Visible has been used. Figure 14 displays the UV–visible absorption spectra before and following 24-h of dipping mild steel in the studied medium including the three inhibitors. The pre-dipping spectra shows that the entire UV–visible wavelengths range between

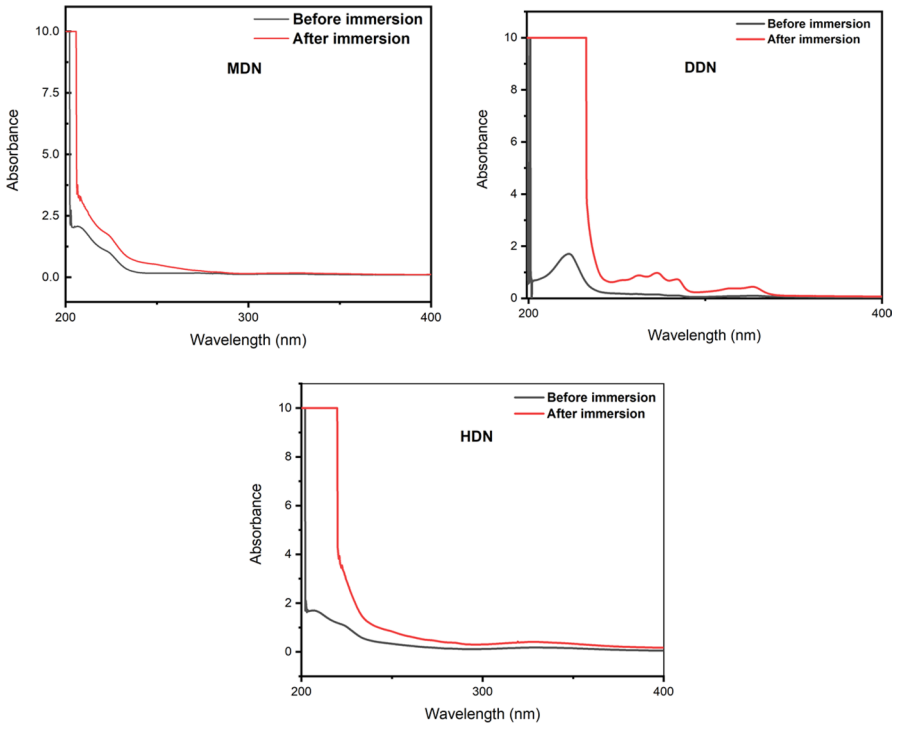

Fig. 14 UV–Vis plots of the concerned system

$\lambda_{max} = 208$ nm and $\lambda_{max} = 223$ nm, this behavior is possibly consistent with aromatic electrons transition π-π* of the under-study inhibitors. However, as can be evident from Fig. 14, the wavelength of absorption shifted to less intense values after 24 h of immersing. More precisely, at subsequent bands at 224.4 nm, 272.2 nm and 327.7 nm for MDN, DDN and HDN probably corresponding to the n-π* pertaining to the heterocyclic ring transition of the investigated species [73]. Typically, according to the literature the change in absorbance (A) value and/or shift of the wavelength (max) indicate the development of a complex between the two chemical compounds in the electrolyte [74]. Our findings verify this attribute, revealing that the investigated inhibitors' heterocyclic rings and aromatic electrons interacted with Fe^{2+} to generate complexes [75].

SEM/EDX investigation

Surface analysis which is a valuable supplement was used to test the pitting endurance of the metal interacting with chloride ions $H^+ + Cl^-$ in the absence and presence of the selected molecules. The results of the precedent study are powerfully supported by the investigation of mild steel's surface morphology. The SEM images tend to convincingly illustrate the inhibitory efficiency in forming a protective covering. SEM images and related EDX spectra of MS in in the corrosive medium without and with inclusion of 0.1 mM of MDN, DDN, and HDN are displayed in Fig. 15 following 24 h of submersion. It appears that the MS surface plunged in the corrosive media has been severely damaged in the absence of the organic molecules, indicating a potent metal degradation [63]. The presence of the ligands under tough circumstances results in their adherence to the alloy's surface, coating the exposed part and minimizing the amount of rust on the samples. [76]. The elements (C, N, O, and Fe) can be observed in peak form the EDS spectra of the MS samples. All the species contained in the inhibitor molecules are represented as peaks in the MS spectrum when diazenyl naphthalen analogues are present, indicating that the molecules under examination have adhered to the steel surface. These results are consistent with the fact that MDN, DDN, and HDN derivatives prevented corrosion in steel through the development of a layer that minimized electrolyte contact with the steel surface [77]. The occurrence of nitrogen atoms, aromatic rings in the molecular skeleton, and functional groups alcohol (OH) and ester (CO_2CH_3) are thought to be involved to the adhesion of the compounds under investigation on the surface of steel [78].

Proposed adsorption process

The primary factor determining the resistance to corrosion exhibited by an inhibitor was its adsorptive affinity at the steel/solution interface, which results in the creation of a protective coating on the metal which prevents its surface exposure to the corrosive media [79]. In fact, the inhibitor compounds were totally ionized by HCl solutions, which produced a number of cations and anion. The original water molecules were subsequently replaced by these ions, which were adsorbed

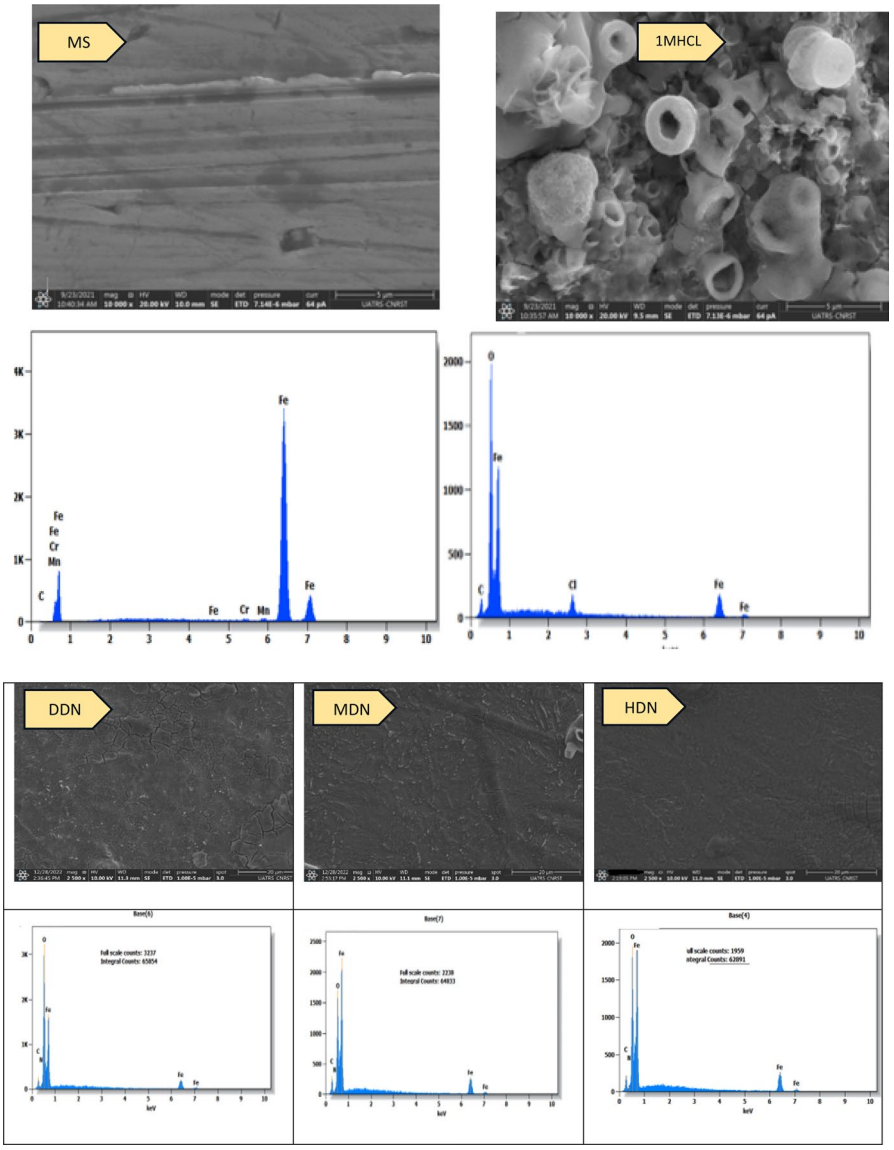

Fig. 15 SEM and EDX graphs of the concerned system

onto the mild steel surface, preventing the corrosive medium from attacking the metal surface [22]. The comparison of adsorption process of the studied diazenyl naphthalen molecules MDN, DDN and HDN was considered to have many physicochemical aspects, such as steric, aromaticity, geometry, functional groups with donor atoms, π-orbital of the donating group, and the molecular weight [20]. The presence of unshared electron pairs on hetero atoms and π -electrons of aromatic rings may be argued to be responsible for the adsorption of DDN on the C-steel

surface. Beyond that, it is demonstrated that the MDN ligand has a significantly higher capacity to prevent corrosion than HDN and DDN, considering the existence of an ester functional group in MDN molecular structure which enhances chemical adsorption. In fact, this privilege is owed to the presence of CO_2CH_3 exhibiting mesomeric effect—M in ortho position in the molecular structure, this imparts the molecule the character of electron donor, which may facilitate further interaction with the metallic surface [80]. Consequently, the adsorption ability of MDN is influenced positively. However, the cyanide group in the HDN compound are positioned in para position, which reduces slightly the possibility of efficient interaction with the metal surface at low concentrations compared to MDN. Considering the outcomes, we suggest the adsorption mechanism illustrated in Fig. 16. Around anodic sites, Cl^- ions were first adsorbed. After then, physical adsorption occurred because of the cations getting attracted to the anions by electrostatic contact. The cations and anions produced an adsorptive layer by replacing the initial water molecules. On the other hand, in the cathodic sites, the cations may compete with hydrogen ions for spots to adsorb and available electrons, which would prevent the hydrogen evolution reaction from occurring. Furthermore, following the assimilation of an electron, the cations may change into their neutral state and favoring the chemisorption due to the existence of heteroatoms' free electron pair and the π electron on the heterocyclic ring. In addition, the cation form can chemically be incorporated onto the surface of the MS by interacting as a donor and acceptor between heteroatoms' free electron pairs (N, O) and the accessible d-orbital on the MS surface. Also, the donor/acceptor interaction between the surface's iron atoms' d-orbitals and the anti-bonding molecular orbitals of the ligands engaged in this adsorption process [28].

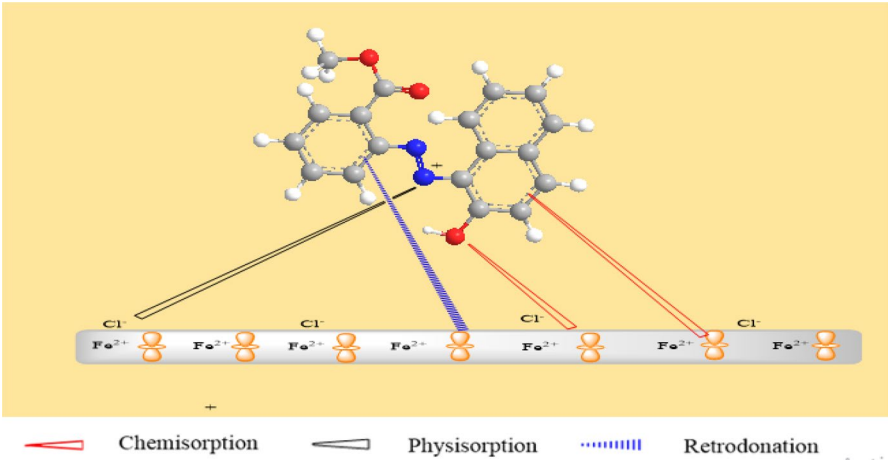

Fig. 16 Inhibition mechanism of the concerned system

Conclusion

The anti-corrosive performance and inhibition process of diazenyl naphthalen analogues toward CS corrosion in an acidic medium has been evaluated employing a systemic approach and analytical means, the ligands demonstrated very high corrosion inhibition efficacy. Potentiodynamic polarization confirms the mixed type nature of inhibitors by showing a drop in the cathodic hydrogen evolution reaction and the anodic metal dissolution, leading to a considerable decrease in corrosion current densities. The creation of a protective layer at the metal/solution interface is confirmed by electrochemical impedance spectroscopy, which further demonstrates that the transfer of charge is mainly the cause of mild steel corrosion. The inhibitory efficiency is greater than 89% for all temperature ranges, demonstrating the usefulness of inhibitors at elevated temperatures. Strong chemical sorption that conforms to the Langmuir isotherm model ensures the investigated inhibitor's surface adhesion. The quantum chemistry computation links molecular structures and charge density distributions to the corrosion inhibition efficiency of inhibitors MDN, DDN, and HDN and further establishes that inhibitor MDN's strong inhibition performance results from its strong adsorption capacity.

Acknowledgements This research project was supported by the "Energy Technology Development Project" of the Ministry of Trade, Industry and Energy (MOTIE) and the Korea Institute of Energy Technology Evaluation and Planning (KETEP). (No. 20203010040010). Also, this research project was supported by the "New and Renewable Energy Core Technology Development Project" of the Ministry of Trade, Industry and Energy (MOTIE) and the Korea Institute of Energy Technology Evaluation and Planning (KETEP). (No. 2022303004020A). In addition, this research was also project was supported by the "Energy Technology Development Project" of the Ministry of Trade, Industry and Energy (MOTIE) and the Korea Institute of Energy Technology Evaluation and Planning (KETEP). (No. 00234839).

Author contributions **Selma Lamghafri and Walid Daoudi** contributed to the writing, formal analysis, and investigation; **Abdelmalik El Aatiaoui, Omar Dagdag, Asma Barrahi, and Avni berisha** were involved in writing, formal analysis, investigation, and supervision; **Souheyla Chetioui and Amel Djedouani** assisted in the conceptualization; **Abdelkader Zarrouk** performed the review and editing; **Abdellatif Lamhamdi** was involved in the supervision.

Funding This research received no external funding.

Data availability No datasets were generated or analyzed during the current study.

Declarations

Conflict of interest The authors declare no competing interests.

Ethical approval There are no prospective studies on humans in this paper.

Consent for publication All authors have consent for publication of this manuscript.

References

1. H.A. Soliman, M.M. Ibrahim, L.I. Ali, M. Saif, N.S. Abdelshafi, K.F. Khaled, Moroc. J. Chem. **11**(3), 11 (2023)
2. O.S.I. Fayomi, I.G. Akande, S. Odigie, J. Phys. Conf. Ser. **1378**, 022037 (2019)
3. F. Bentiss, M. Traisnel, M. Lagrenee, Corros. Sci. **42**, 127 (2000)
4. S. Lamghafri, W. Daoudi, A.E. Aatiaoui, O. Dagdag, H. Kim, A. Berisha, W.B.W. Nik, A.J. Obaidullah, K.K. Yadav, A. Zarrouk, A. Lamhamdi, J. Mol. Struct. **1306**, 137924 (2024)
5. N. Idlahoussaine, M. Lasri, R. Idouhli, W. Daoudi, B. EL Ibrahimi, E. Berdimurodov, M. El ouardi, A. A. Addi, N. Aliev, A. E. Aatiaoui, A. Abouelfida, J. Mol. Struct. **1305,** 137705 (2024)
6. E.A. Noor, Corros. Sci. **47**, 33 (2005)
7. M. El Faydy, F. Benhiba, Y. Kerroum, A. Guenbour, F. Bentiss, I. Warad, B. Lakhrissi, A. Zarrouk, J. Mol. Liq. **325**, 115224 (2021)
8. R.S. Abdel-Hameed, O.E. El-Azabawy, A.A. El-Segaey, E.A. Khamis, N.S. Abdelshafi, H.I. Al-Shafey, Can. Metall. Q. **01**, 1 (2023)
9. N.S. Abdelshafi, M.A. Sadik, M.A. Shoeib, S.A. Halim, Arab. J. Chem. **15**, 103459 (2022)
10. T.H. El-Mokadem, A.I. Hashem, N.E.A. Abd El-Sattar, E.A. Dawood, N.S. Abdelshafi, J. Mol. Struct. **1274**, 134567 (2023)
11. F. Benhiba, M. Missioui, S. Lamghafri, R. Hsissou, A. Bellaouchou, H. Oudda, A. Lamhamdi, I. Warad, Y. Ramli, A. Zarrouk, Coatings **13**, 1109 (2023)
12. M.A. Dawood, Int. J. Corros. Scale Inhib. **10**, 1766 (2021)
13. F.E. Hajjaji, R. Salim, E. Ech-chihbi, A. Titi, M. Messali, S. Kaya, B.E. Ibrahimi, M. Taleb, J. Taiwan Inst. Chem. Eng. **123**, 346 (2021)
14. A. Saady, E. Ech-chihbi, F. El-Hajjaji, F. Benhiba, A. Zarrouk, Y.K. Rodi, M. Taleb, A. El Biache, Z. Rais, J. Appl. Electrochem. **51**, 245 (2021)
15. W. Daoudi, A. El Aatiaoui, S. Lamghafri, A. Oussaid, A. Oussaid, *Phytochemicals in Medicinal Plants: Biodiversity, Bioactivity and Drug Discovery,* ed. by C. Arora, D. K. Verma, J. Aslam, P. K. Mahish (De Gruyter, 2023), p. 227
16. J. Amoko, O. Akinyele, D. Olayanju, A. Oluwafemi, and C. Aboluwoye, (n.d.).
17. O.F. Akinyele, A.S. Adekunle, D.S. Olayanju, O.E. Oyeneyin, S.S. Durodola, N.D. Ojo, A.A. Akinmuyisitan, T.A. Ajayeoba, L.O. Olasunkanmi, J. Mol. Struct. **1268**, 133738 (2022)
18. E. Akroujai, S. Chetioui, N. Benzbiria, A. Barrahi, A. Chraka, A. Djedouani, S. Chtita, S. Lazar, I. Warad, A. Bellaouchou, M. Assouag, A. Zarrouk, Int. J. Corros. Scale Inhib. **12**, 1102 (2023)
19. H.T. Obaid, M.Y. Kadhum, A.S. Abdulnabi, Mater. Today Proc. **60**, 1394 (2022)
20. A.S. Fouda, M.A. El-morsi, M. Gaber, M. Fakeeh, Chem. Data Collect. **28**, 100479 (2020)
21. A. Elsamman, K.F. Khaled, S.A. Halim, N.S. Abdelshafi, J. Mol. Struct. **1297**, 136728 (2024)
22. H.R. Obayes, A.A. Al-Amiery, G.H. Alwan, T.A. Abdullah, A.A.H. Kadhum, A.B. Mohamad, J. Mol. Struct. **1138**, 27 (2017)
23. G. Gao, C. Liang, Electrochim. Acta **52**, 4554 (2007)
24. F. Benhiba, R. Hsissou, Z. Benzekri, M.E. Belghiti, A. Lamhamdi, A. Bellaouchou, A. Guenbour, S. Boukhris, H. Oudda, I. Warad, A. Zarrouk, J. Mol. Liq. **312**, 113367 (2020)
25. D. Costa, T. Ribeiro, P. Cornette, P. Marcus, J. Phys. Chem. C **120**, 28607 (2016)
26. H. Wang, X. Wang, H. Wang, L. Wang, A. Liu, J. Mol. Model. **13**, 147 (2006)
27. W. Daoudi, L. Guo, M. Azzouzi, T. Pooventhiran, A.E. Boutaybi, S. Lamghafri, A. Oussaid, A. El Aatiaoui, J. Adhes. Sci. Technol. **37**, 2944 (2023)
28. S. Lamghafri, W. Daoudi, A. El Aatiaoui, O. Dagdag, A. Berisha, A. Barrahi, W.B. Wan Nik, A. Zarrouk, A. Lamhamdi, Mater. Sci. Eng. B **297**, 116779 (2023)
29. W. Daoudi, M. Azzouzi, O. Dagdag, A. El Boutaybi, A. Berisha, E.E. Ebenso, A. Oussaid, A. El Aatiaoui, Mater. Sci. Eng. B **290**, 116287 (2023)
30. D.K. Verma, E.E. Ebenso, M.A. Quraishi, C. Verma, Results Phys. **13**, 102194 (2019)
31. A.E. Aatiaoui, M. Koudad, T. Chelfi, S. Erkan, M. Azzouzi, A. Aouniti, K. Savaş, M. Kaddouri, N. Benchat, A. Oussaid, J. Mol. Struct. **1226**, 129372 (2021)
32. A.A. Farag, E.A. Mohamed, G.H. Sayed, K.E. Anwer, J. Mol. Liq. **330**, 115705 (2021)
33. A. Saady, Z. Rais, F. Benhiba, R. Salim, K. Ismaily Alaoui, N. Arrousse, F. Elhajjaji, M. Taleb, K. Jarmoni, Y. Kandri Rodi, I. Warad, A. Zarrouk, Corros. Sci. **189**, 109621 (2021)
34. K.E. Anwer, A.A. Farag, E.A. Mohamed, E.M. Azmy, G.H. Sayed, J. Ind. Eng. Chem. **97**, 523 (2021)

35. A. Zarrouk, I. El Ouali, M. Bouachrine, B. Hammouti, Y. Ramli, E.M. Essassi, I. Warad, A. Aouniti, R. Salghi, Res. Chem. Intermed. **39**, 1125 (2013)
36. W. Zhang, B. Nie, H.-J. Li, Q. Li, C. Li, Y.-C. Wu, Carbohydr. Polym. **260**, 117842 (2021)
37. M. Abdallah, Corros. Sci. **44**, 717 (2002)
38. I. Ahamad, R. Prasad, M.A. Quraishi, Corros. Sci. **52**, 1472 (2010)
39. J.O.M. Bockris, S. Srinivasan, J. Electrochem. Soc. **111**, 858 (1964)
40. A. Berisha, Electrochem **1**, 188 (2020)
41. A. Ghazoui, R. Saddik, N. Benchat, B. Hammouti, M. Guenbour, A. Zarrouk, R. Mohammed, Pharma Chem. **4**, 352 (2012)
42. M.S.S. Carranza, Y.I.A. Reyes, E.C. Gonzales, D.P. Arcon, F.C. Franco, Heliyon **7**, 07952 (2021)
43. R. Salim, E. Ech-Chihbi, H. Oudda, Y. ELAoufir, F. El-hajjaji, E. Abdelmalik, A. Oussaid, B. Hammouti, H. Elmsellem, M. Taleb, Pharma Chem. **8**, 200 (2016)
44. S. Bourichi, Y. Kandri Rodi, M. el Azzouzi, Y. Kharbach, O. Fouad, A. Aouniti, J. Mater. Environ. Sci. **8**, 1696 (2017)
45. D.B. Hmamou, R. Salghi, A. Zarrouk, H. Zarrok, B. Hammouti, S.S. Al-Deyab, A.E. Assyry, N. Benchat, M. Bouachrine, Int. J. Electrochem. Sci. **8**, 20 (2013)
46. W. Daoudi, S. Lamghafri, O. Dagdag, R. Haldhar, and A. E. Aatiaoui, (n.d.).
47. N.S. Abdelshafi, M.A. Ibrahim, A.-S. Badran, S.A. Halim, J. Mol. Struct. **1250**, 131750 (2022)
48. A. Elsamman, K.F. Khaled, S.A. Halim, N.S. Abdelshafi, J. Mol. Struct. **1293**, 136230 (2023)
49. A. Ghazoui, R. Saddik, B. Hammouti, A. Zarrouk, N. Benchat, M. Guenbour, S.S. Al-Deyab, I. Warad, Res. Chem. Intermed. **39**, 2369 (2013)
50. B.D. Mert, A.O. Yüce, G. Kardaş, B. Yazıcı, Corros. Sci. **85**, 287 (2014)
51. R. Yıldız, A. Döner, T. Doğan, İ Dehri, Corros. Sci. **82**, 125 (2014)
52. A.A. Al-Amiery, L.M. Shaker, KOM – Corros. Mater. Prot. J. **64**, 59 (2020)
53. E. Ech-chihbi, A. Nahlé, R. Salim, H. Oudda, F. El Hajjaji, F. El Kalai, A. El Aatiaoui, M. Taleb, J. Bio- Tribo-Corros. **5**, 24 (2019)
54. N. Bensalah, *Pitting Corrosion (BoD – Books on Demand)* (InTech, 2012)
55. A.R. Shahmoradi, M. Ranjbarghanei, A.A. Javidparvar, L. Guo, E. Berdimurodov, B. Ramezanzadeh, J. Mol. Liq. **338**, 116550 (2021)
56. M. Mobin, I. Ahmad, M. Shoeb, J. Adhes. Sci. Technol. **36**, 2562 (2022)
57. A.M. Beccaria, G. Poggi, M. Arfelli, G. Mattogno, Corros. Sci. **34**, 989 (1993)
58. A. Benzai, F. Derridj, O. Mouadili, M. Azzouzi, M. Kaddouri, K. Cherrak, R. Touzani, A. Aouniti, B. Hammouti, R. Elatki, H. Doucet, Port. Electrochimica Acta **39**, 135 (2021)
59. C.S. Varghese, K.J. Thomas, V.P. Raphael, K.S. Shaju, Curr. Chem. Lett. **8**, 1 (2019)
60. B. El Mehdi, B. Mernari, M. Traisnel, F. Bentiss, M. Lagrenée, Mater. Chem. Phys. **77**, 489 (2003)
61. A.A. El-Awady, B.A. Abd-El-Nabey, S.G. Aziz, J. Electrochem. Soc. **139**, 2149 (1992)
62. I.B. Obot, I.B. Onyeachu, A.M. Kumar, Carbohydr. Polym. **178**, 200 (2017)
63. E. Ituen, O. Akaranta, A. James, Chem. Sci. Int. J. **18**, 1 (2017)
64. J. Wang, X. Guo, Chemosphere **258**, 127279 (2020)
65. I. Lukovits, E. Kálmán, G. Pálinkás, Corrosion **51**, 201 (1995)
66. S.O. Adejo, M.M. Ekwenchi, J.A. Gbertyo, T. Menengea, J.O. Ogbodo, J. Adv. Chem. **10**, 2737 (2014)
67. K.Y. Foo, B.H. Hameed, Chem. Eng. J. **156**, 2 (2010)
68. M. Christov, A. Popova, Corros. Sci. **46**, 1613 (2004)
69. W. Durnie, R. De Marco, A. Jefferson, B. Kinsella, J. Electrochem. Soc. **146**, 1751 (1999)
70. M. Cui, S. Ren, H. Zhao, L. Wang, Q. Xue, Appl. Surf. Sci. **443**, 145 (2018)
71. K. Qu, J. Wang, J. Ren, X. Qu, Chem. Eur. J. **19**, 7243 (2013)
72. A. Zouitini, Y.K. Rodi, H. Elmselem, F.O. Chahdi, H. Steli, C. Ad, E.M. Essassi, A. Chetouani, B. Hammouti, Moroccan J. Chem **6**, 391 (2018)
73. J.A. Pereira, A.M. Pessoa, M.N.D.S. Cordeiro, R. Fernandes, C. Prudêncio, J.P. Noronha, M. Vieira, Eur. J. Med. Chem. **97**, 664 (2015)
74. M.H. Shahini, M. Ramezanzadeh, G. Bahlakeh, B. Ramezanzadeh, J. Mol. Liq. **332**, 115876 (2021)
75. C. Verma, M.A. Quraishi, E.E. Ebenso, Surf. Interfaces **21**, 100634 (2020)
76. F. Bentiss, M. Traisnel, H. Vezin, H.F. Hildebrand, M. Lagrenée, Corros. Sci. **46**, 2781 (2004)
77. S.S. Abd El Rehim, S.M. Sayyah, M.M. El-Deeb, S.M. Kamal, R.E. Azooz, Int. J. Ind. Chem. **7**, 39 (2016)

78. A. Popova, E. Sokolova, S. Raicheva, M. Christov, Corros. Sci. **45**, 33 (2003)
79. P. Mourya, P. Singh, A.K. Tewari, R.B. Rastogi, M.M. Singh, Corros. Sci. **95**, 71 (2015)
80. S. Lamghafri, Mater. Sci. **297**, 116779 (2023)

Authors and Affiliations

Selma Lamghafri[1] · Souheyla Chetioui[2,3] · Asma Barrahi[4] · Walid Daoudi[5] · Omar Dagdag[6] · Abdelmalik El Aatiaoui[5] · Avni Berisha[7] · Amel Djedouani[8,9] · Abdelkader Zarrouk[4] · Abdellatif Lamhamdi[1]

✉ Walid Daoudi
walid.daoudi@ump.ac.ma

✉ Avni Berisha
avni.berisha@uni-pr.edu

1 Laboratory of Applied Sciences, National School of Applied Sciences Al-Hoceima, Abdelmalek Essaadi University, Tetouan, Morocco

2 Faculty of Technology, University of M'sila, PO Box 166 Ichebilia, 28000 M'sila, Algeria

3 Research Unit for Chemistry of the Environment and Molecular Structural, University of Constantine 1, 25000 Constantine, Algeria

4 Laboratory of Materials, Nanotechnology and Environment, Faculty of Sciences, Mohammed V University in Rabat, P.O. Box. 1014, Rabat, Morocco

5 Laboratory of Molecular Chemistry, Materials and Environment (LCM2E), Department of Chemistry, Multidisciplinary Faculty of Nador, University Mohamed I, 60700 Nador, Morocco

6 Department of Mechanical Engineering, Gachon University, Seongnam 13120, Republic of Korea

7 Department of Chemistry, Faculty of Natural and Mathematics Science, University of Prishtina, 10000 Prishtina, Kosovo

8 Department of Physics and Chemistry, Ecole Normale Superior Assia Djebar of Constantine, University Constantine 3, 25000 Constantine, Algeria

9 Laboratory of Analytical Physicochemistry and Crystallochemistry of Organometallic and Biomolecular Materials, University Constantine 1, 25000 Constantine, Algeria

Terms and Conditions

Springer Nature journal content, brought to you courtesy of Springer Nature Customer Service Center GmbH ("Springer Nature").

Springer Nature supports a reasonable amount of sharing of research papers by authors, subscribers and authorised users ("Users"), for small-scale personal, non-commercial use provided that all copyright, trade and service marks and other proprietary notices are maintained. By accessing, sharing, receiving or otherwise using the Springer Nature journal content you agree to these terms of use ("Terms"). For these purposes, Springer Nature considers academic use (by researchers and students) to be non-commercial.

These Terms are supplementary and will apply in addition to any applicable website terms and conditions, a relevant site licence or a personal subscription. These Terms will prevail over any conflict or ambiguity with regards to the relevant terms, a site licence or a personal subscription (to the extent of the conflict or ambiguity only). For Creative Commons-licensed articles, the terms of the Creative Commons license used will apply.

We collect and use personal data to provide access to the Springer Nature journal content. We may also use these personal data internally within ResearchGate and Springer Nature and as agreed share it, in an anonymised way, for purposes of tracking, analysis and reporting. We will not otherwise disclose your personal data outside the ResearchGate or the Springer Nature group of companies unless we have your permission as detailed in the Privacy Policy.

While Users may use the Springer Nature journal content for small scale, personal non-commercial use, it is important to note that Users may not:

1. use such content for the purpose of providing other users with access on a regular or large scale basis or as a means to circumvent access control;
2. use such content where to do so would be considered a criminal or statutory offence in any jurisdiction, or gives rise to civil liability, or is otherwise unlawful;
3. falsely or misleadingly imply or suggest endorsement, approval , sponsorship, or association unless explicitly agreed to by Springer Nature in writing;
4. use bots or other automated methods to access the content or redirect messages
5. override any security feature or exclusionary protocol; or
6. share the content in order to create substitute for Springer Nature products or services or a systematic database of Springer Nature journal content.

In line with the restriction against commercial use, Springer Nature does not permit the creation of a product or service that creates revenue, royalties, rent or income from our content or its inclusion as part of a paid for service or for other commercial gain. Springer Nature journal content cannot be used for inter-library loans and librarians may not upload Springer Nature journal content on a large scale into their, or any other, institutional repository.

These terms of use are reviewed regularly and may be amended at any time. Springer Nature is not obligated to publish any information or content on this website and may remove it or features or functionality at our sole discretion, at any time with or without notice. Springer Nature may revoke this licence to you at any time and remove access to any copies of the Springer Nature journal content which have been saved.

To the fullest extent permitted by law, Springer Nature makes no warranties, representations or guarantees to Users, either express or implied with respect to the Springer nature journal content and all parties disclaim and waive any implied warranties or warranties imposed by law, including merchantability or fitness for any particular purpose.

Please note that these rights do not automatically extend to content, data or other material published by Springer Nature that may be licensed from third parties.

If you would like to use or distribute our Springer Nature journal content to a wider audience or on a regular basis or in any other manner not expressly permitted by these Terms, please contact Springer Nature at

onlineservice@springernature.com